The climate response to multiple volcanic eruptions mediated by ocean heat uptake: damping processes and accumulation potential

Mukund Gupta & John Marshall

Department of Earth, Atmospheric, and Planetary Sciences,

Massachusetts Institute of Technology, Cambridge, MA 02139

Email: guptam@mit.edu

Abstract

A hierarchy of models is used to explore the role of the ocean in mediating the response of the climate to a single volcanic eruption and to a series of eruptions by drawing cold temperature anomalies in to its interior, as measured by the ocean heat exchange parameter q [$Wm^{-2}K^{-1}$]. The response to a single (Pinatubo-like) eruption comprises two primary timescales, one fast (year) and one slow (decadal). Over the fast timescale, the ocean sequesters cooling anomalies induced by the eruption in to its depth, enhancing the damping rate of sea surface temperature (SST) relative to that which would be expected if the atmosphere acted alone. This compromises the ability to constrain atmospheric feedback rates measured by λ [~ 1 $Wm^{-2}K^{-1}$] from study of the relaxation of SST back toward equilibrium, but yields information about the transient climate sensitivity proportional to $\lambda + q$. Our study suggests that q can significantly exceed λ in the immediate aftermath of an eruption but becomes smaller as time progresses. Shielded from damping to the atmosphere, the effect of the volcanic eruption persists on longer decadal timescales. Finally, we assess the 'accumulation potential' of a succession of volcanic eruptions over time, a process that may in part explain the prolongation of cold surface temperatures experienced during, for example, the Little Ice Age.

1. Introduction

Large volcanic eruptions are a natural, impulse-like perturbation to the climate system. The sulfur particles ejected into the stratosphere during eruptions are rapidly converted to sulfate aerosols that diminish the net incoming solar flux at the top of the atmosphere resulting in a cooling of the surface climate. These sulfate aerosols have a long residence time of about 1-2 years in the stratosphere (Robock, 2000) but can cause surface cooling for many more years after the eruption.

The response of the climate to volcanic eruptions is of interest for at least two reasons. First, it can teach us about how robust is the climate to a perturbation and the rate at which it relaxes back to equilibrium (see, e.g. Wigley et al. 2005, Bender et al. 2010, Merlis et al. 2014). Second, because of its large effective heat capacity, the ocean can perhaps remember the effect of successive eruptions, enabling an accumulation larger than any single event (see, e.g. Free et al. 1999, Crowley et al. 2008, Stenchikov et al. 2009). Some of the issues are illustrated in Fig.1, which shows the hypothetical response of the climate to a volcanic eruption in two limit cases. In the first, the atmosphere is imagined to be coupled to a slab ocean. The relaxation of the system here depends simply on the climatic feedback parameter λ [$Wm^{-2}K^{-1}$] and the slab's heat capacity. The larger the value of λ, the smaller the equilibrium climate sensitivity and the faster the system relaxes back to equilibrium. In the second, the slab lies atop an interior ocean that can sequester heat away from the surface at a rate proportional to the ocean heat exchange parameter q [$Wm^{-2}K^{-1}$], enhancing damping of the surface temperature in the initial stages. However, on longer timescales, the sequestered heat anomaly is shielded from damping to space leading to a prolongation of the signal. Thus, interaction with the interior ocean changes the response from that of a simple exponential decay on one timescale to a two-timescale process, as evidenced by the ‘dog-leg’ profile evident in Fig.1 which becomes more prominent as the ratio $\mu = q/\lambda$ increases.

Many studies have explored the role of the subsurface ocean in the climatic response to external forcings (e.g. Hansen et al. 1985; Gregory 2000; Stouffer 2004; Winton et al 2010; Held et al. 2010; Geoffroy et al. 2013). Volcanic responses have been explored in simple box models (e.g. Lindzen and Giannitsis 1998) as well as in state-of-the-art global climate models and observations (e.g. Church et al. 2005; Glecker et al. 2006; Stenchikov et al. 2009; Merlis et al. 2014; Schurer et al. 2015). Here, we explore the role of the ocean in sequestering thermal anomalies to depth and enhancing initial surface damping rates, while temporarily shielding those anomalies from damping processes and thereby extending the response timescale. As we shall see, this mechanism can promote accumulation of the cooling signal from successive eruptions and cause the response to span multi-decadal timescales. While previous studies (e.g. Geoffroy et al. 2013; Kostov et al. 2013) have reported $\mu \sim 1$, we argue that over relatively short timescales (years to a decade or so), μ can be considerably larger than 1. We explore the consequences for estimating λ in the immediate aftermath of a volcanic eruption from the relaxation timescale of SST. We also quantify the role of the interior ocean in extending the response from volcanic eruptions.

Our study employs a hierarchy of idealized models - ranging from a 2-box model, a 1-D diffusion model and a coupled Global Circulation Model (GCM). Section 2 explores results from idealized volcanic eruptions in a GCM. In Section 3, we interpret those results using a simple 2-box model of the ocean and investigate the role of μ. In Section 4, we apply the resulting insights to study the climate response to a series volcanic eruptions during the last millennium. In Section 5 we conclude.

2. Experiments with an idealized coupled aquaplanet model

2.1 Experiment description

We use a coupled atmosphere-ocean model based on the MITgcm aquaplanet model (see Appendix A). The model simulates the physics of an ocean-covered planet coupled to an atmosphere, with no land, sea-ice or clouds. Geometrical constraints are imposed on the ocean circulation through the effect of two narrow barriers extending from the North Pole to 35°S and set 90° apart. These barriers extend from the seafloor (assumed flat) to the surface and separate the ocean into a large and a small basin that are connected in a circumpolar region to the south. Despite the simplicity of the geometry, this 'double-drake' configuration captures aspects on the present climate, including plausible energy transports by the oceans and atmosphere, and a deep meridional overturning circulation that is dominated by the small basin (Ferreira et al. 2009).

The atmospheric component of the model employs a simplified radiation scheme where the shortwave flux does not interact with the atmosphere and hence the planetary albedo is equivalent to the surface albedo, as described in Frierson et al. (2006). Idealized volcanic eruptions are simulated by reducing the net incoming shortwave radiative flux by a uniform amount over the globe, while ensuring that it does not become negative anywhere. The forcing is applied as a 1-year square pulse in time starting January 1st. Both single and multiple pulses (separated by a specified interval) are considered. In order to isolate the role of the interior ocean, numerical experiments are run using the 'full ocean' configuration of the MITgcm, as well as a 'slab ocean' configuration that has a single vertical layer representing the annual-mean mixed-layer depth of the model. In the 'slab ocean', a prescribed lateral flux of heat in the mixed layer helps to maintain a climatological SST close to that of the coupled system.

2.2 Idealized volcanic responses

Fig. 2 shows the globally-averaged sea surface temperature (SST) response of the MITgcm to a forcing of -4 Wm^{-2} for 1 year, which crudely emulates the radiative effect of the 1991 Mount Pinatubo eruption. A theoretical 10 × Pinatubo eruption was also simulated using a forcing of -40 Wm^{-2} for a year. Ensemble members (5 for the Pinatubo forcing and 1 for the 10 × Pinatubo forcing) were initialized from a long control integration of the model separated by 10-year intervals. Anomalies were calculated by subtracting the response of the forced run from the control run. Fig. 2 (a) shows all model responses normalized with respect to their peak cooling value. The slab ocean curves decay over a single e-folding timescale of about 4 years, whereas the full ocean curve displays an initial fast relaxation rate and a long-lasting tail (5-10% of the signal present after 20 years). The shape of these response functions are interpreted using a 2-box model of the climate in Section 3.

Fig. 2 (b) shows that in the Pinatubo-like simulations, the SST anomaly reaches a minimum value of -0.62 °C for the slab and -0.41 °C for the full ocean. This difference is the result of some of the cooling being sequestered into the deeper ocean in the case of a dynamic ocean, as argued in Held et al. (2010). Soden et al. (2000) report an observed globally-averaged tropospheric temperature anomaly of -0.5°C the year after the Pinatubo eruption, broadly in accord with our calculations. The shading in Fig. 2 (b) is the envelope corresponding to the response of the various ensemble members, whereas the dotted lines are the ensemble means. In the first year, while the forcing is active, the behavior of each ensemble member shows very little variability, but the simulations diverge from each other after the forcing is turned off. The standard deviation in the SST anomaly eventually settles to 0.11°C for the full ocean and 0.06°C for the slab ocean, characteristic of the noise levels in these configurations. Fig. 2 (c) shows that for a 10 × Pinatubo forcing, the slab ocean displays a maximum cooling of -6.1°C compared to only -3.7°C for the full ocean. This peak cooling scales linearly with the forcing amplitude in the slab ocean case, but is 10% smaller than linear scaling when the ocean is active. This non-linearity can be explained by the fact that the larger forcing causes the mixed layer to deepen, which allows the cooling signal to penetrate further down into the ocean.

As evidenced in Fig. 2 (b), natural variability can readily obscure the response to volcanic eruptions. To explore this issue, we conduct a statistical analysis of the globally and annually-averaged SST in long control simulations of the slab and full ocean configurations. The full ocean simulations shows more variability than those of the slab, due to the many additional degrees of freedom imparted by the presence of a dynamic ocean. Based on a single-sided student's t-test, we find that the slab ocean response in the 10×Pinatubo simulation is significant for 15 years at -0.13°C, whereas the full ocean response remains significant for 22 years at -0.18°C (both at a 95% confidence level). However, for Pinatubo-like events, we require a large number of ensembles (~10) to tease out a significant response for 10-20 years. While noise levels may be different in the real ocean, our analysis suggests that natural variability poses severe limitations on our ability to detect climate SST signals resulting from volcanic eruptions, except, perhaps, for the most significant events such as Santa María, Mount Agung, El Chichón and Mount Pinatubo during the recent historical past.

Fig. 3 shows the evolution of the ocean temperature anomaly as a function of latitude and depth for the Pinatubo and 10×Pinatubo forcings (full ocean configuration). Within 2 years of the eruption, a significant amount of cooling is transported below the mixed layer. Temperature anomalies on the order of 10% of the peak surface cooling exist at 200m depth and persist for more than 10 years after the cooling pulse. A combination of processes may be acting to spread the anomaly vertically, such as turbulent diffusion, Ekman pumping, seasonal convection, mixing in the wind-driven gyres and large scale overturning circulation (e.g. Gregory 2000; Stouffer et al. 2004; Stenchikov et al. 2009). Fig. 3 reveals signatures of Ekman pumping within the subtropical gyres, particularly visible for the 10×Pinatubo forcing. At the poles, the penetration of the anomaly to depth happens over a longer timescale than in mid-latitudes. Several studies (e.g. Stenchikov et al. 2009; Otterå et al. 2010 and Mignot et al. 2011) discuss a strengthening of the meridional overturning circulation in response to volcanic eruptions, which can also contribute to the vertical exchange. For the 10×Pinatubo eruption, the globally-averaged mixed layer depth increases by about 50% (63m) in the year of the eruption and relaxes back to its base value (43m) within 3 years. This increase occurs principally in the mid-latitudes, where most of the anomalous subduction of cooling occurs in the first few years after the eruption. This might explain the slight non-linearity in the 10×Pinatubo response visible in Fig. 2 and mentioned above.

Fig. 4 shows simulations of a series of Pinatubo-like eruptions occurring every 10 years in the slab and full ocean configurations. In the slab ocean case, the response falls back to zero after each eruption. On the other hand, the full ocean response slowly builds up over time, as seen by the 20% increase in peak cooling achieved 60 years or so after the first eruption. This suggests that the presence of a deeper ocean can facilitate the build-up of a cooling signal from successive eruptions. In Section 3, we discuss the conditions that can lead to signal accumulation using a 2-box model as a guide.

3. Interpretation using a 2-box model

3.1 The two-timescale response

The globally-averaged SST responses of the MITgcm aquaplanet to an idealized volcanic forcing can be interpreted using simple analytical models. We find that the shapes of the temperature response functions are most readily recovered and interpreted through use of a 2-box model[1]. The model, shown in Fig. 5, was introduced by Gregory (2000) and has subsequently been employed by Held et al. (2010), Geoffroy et al (2013), Kostov et al. (2013) and others. It consists of a mixed layer and a deeper ocean box of temperature T_1 and T_2 respectively, driven from the top by an external forcing F and damped by the climate feedback λT_1. The governing equations can be written as follows:

$$\rho c_w h_1 \frac{dT_1}{dt} = -\lambda T_1 + q(T_2 - T_1) + F(t) \qquad (1)$$

and

$$\rho c_w h_2 \frac{dT_2}{dt} = q(T_1 - T_2), \qquad (2)$$

where h_1 and h_2 are the thicknesses of the mixed layer and deeper ocean boxes respectively. The density and heat capacity of water are ρ and c_w respectively. The parameter q represents vertical ocean heat exchange; it is positive for an active deeper ocean and zero for a slab ocean. We represent an idealized volcanic eruption by imposing a delta function forcing $F(t) = V\delta(t)$ in Eq. (1), where V is the integrated amount of energy instantaneously extracted from the system. This impulse (or Green's function) response provides information on the first order climate response to a volcanic eruption and lends itself to convolution with a more realistic time series of forcing (see Section 4). The analytical solution to Eq. (1) and (2) is presented in the

[1] We have also applied a 1-D diffusion model which, for completeness and the convenience of future researchers, we present in Appendix B. This is less successful at capturing the form of the GCM response than the two-box model.

Supplementary Information (SI) and is consistent with the work of Geoffroy et al. (2013), Kostov et al (2013) and Tsutsui (2017) who wrote down the solution to a step in the forcing. The solution for T_1 is the sum of two decaying exponentials:

$$T_1(t) = T_f e^{-t/\tau_f} + T_s e^{-t/\tau_s} \qquad \text{(3a)} \qquad \text{and} \qquad T_f + T_s = T_c \, , \qquad \text{(3b)}$$

where T_c, T_f, T_s, τ_f and τ_s are written out in the SI, together with the solution for T_2. Eq. (3) describes the relaxation of T_1 back to equilibrium after the forcing F has ceased to act. The relaxation occurs over a fast and a slow timescale with e-folding values τ_f and τ_s respectively. In the case of a delta function forcing, the peak cooling T_c occurs instantaneously at t = 0 and is given by:

$$T_c = \frac{V}{\rho c_w h_1} \, , \qquad (4)$$

where V is the integrated amount of energy extracted from the system by the forcing:

$$V = \int_0^\infty F(t) dt \, . \qquad (5)$$

Eq. (4) suggests that the peak cooling T_c does not depend on the climatic feedback λ and oceanic damping q, but this is only valid for an idealized instantaneous forcing, as will be seen in Section 3.4.

The full analytical solutions are unwieldy and not very informative, but may be simplified by introducing the parameters μ and r:

$$\mu = \frac{q}{\lambda} \qquad \text{(6a)} \qquad \text{and} \qquad r = \frac{h_1}{h_2} \, . \qquad \text{(6b)}$$

The parameter μ represents the ratio of the ocean damping strength versus climatic damping, and r is the ratio of heat capacities between the two boxes. We consider two limiting cases: (i) r is small and (ii) r is small and μ is first small and then large. In Section 3.2, we fit our model to the MITgcm simulations and find that r ~ 1/3 and μ ~ 3, suggesting that the limit of r small and μ large is perhaps the most relevant.

In the SI, we show that in the limit of small r, the parameters τ_f and τ_s & T_f, T_s, are given by:

$$\tau_f \approx \frac{\rho c_w h_1}{\lambda(1+\mu)}, \quad (7a) \qquad \tau_s \approx \rho c_w h_1 \frac{(1+\mu)}{qr}, \quad (7b)$$

$$T_f \approx \frac{(1+\mu)^2}{(1+\mu)^2 + r\mu^2}, \quad (8a) \text{ and } \qquad T_s \approx \frac{r\mu^2}{(1+\mu)^2 + r\mu^2} T_c. \quad (8b)$$

When $\mu \ll 1$, a 1-box model is retrieved. In this case the transfer of heat to the deeper ocean is limited and the atmosphere is the only significant medium responsible for damping the anomaly. The solution reduces to a single exponential decay controlled by damping to the atmosphere:

$$T_1(t) = T_c\, e^{-t/\tau_m}, \quad (9a) \qquad \text{with } \tau_m = \frac{\rho c_w h_1}{\lambda}. \quad (9b)$$

When $\mu \gg 1$, i.e. when ocean heat transport is large relative to damping to the atmosphere, the two-timescale solution becomes:

$$\tau_f \approx \frac{\rho c_w h_1}{q}, \quad (10a) \qquad \tau_s \approx \frac{\rho c_w h_2}{\lambda} = \frac{\mu \tau_f}{r}, \quad (10b)$$

$$T_f \approx \frac{T_c}{1+r}, \quad (11a) \quad \text{and} \qquad T_s \approx \frac{r}{1+r} T_c. \quad (11b)$$

In this limit it is interesting (and curious) to note that the fast timescale is controlled by oceanic damping q, whereas the slow timescale is controlled by the climatic feedback λ. The two timescales lead to the 'dog-leg' profile evident in Fig. 1 which becomes more prominent as the ratio μ increases. Physically, we can understand this as a rapid initial response during which the temperature anomaly is sequestered in the deeper ocean, followed by a slower evolution during which the anomaly is damped by climatic feedbacks. In this limit, the coefficients T_f and T_s only depend on T_c and r. We now go on to assess the magnitudes of r and μ by fitting the analytical solutions to curves obtained from the GCM.

3.2 Parameter fitting for an impulse response

Fig. 6 (a) shows the 1-box and 2-box model fits to the MITgcm slab and full ocean responses respectively. The value of h_1 is set to 43m, the globally and annually-averaged mixed layer depth diagnosed from a long control simulation of the coupled model. To estimate λ, we use the equilibrium response of the slab ocean configuration to a constant, spatially uniform forcing F_s. Setting $F(t) = F_s$ in Eq. (1) produces a response that asymptotes to the equilibrium climate sensitivity (ECS):

$$ECS = \frac{F_s}{\lambda} = -2.67°\text{C}. \qquad (12)$$

for $F_s = -4\ Wm^{-2}$, giving $\lambda = 1.5\ Wm^{-2}K^{-1}$. We then use least-square minimization with respect to the full ocean Pinatubo response in Fig.2 (b) to obtain $q = 3.5\ Wm^{-2}K^{-1}$ and $h_2 = 150$m (and thus r = 0.29 and μ = 2.3) with a fitting accuracy of $R^2 = 0.87$. The fit to the slab ocean configuration ($R^2 = 0.97$) is obtained by setting q = 0. The relaxation time of the slab ocean curve is $\tau_m = 4$ years, whereas the fast and slow timescales corresponding to the full ocean simulations are $\tau_f =$ 1 year and $\tau_s =$ 22 years respectively. Parameter fits are summarized in Table 1, where the goodness of the approximate expressions, Eq. (7) to (11), is assessed by comparison with the full analytical expression. The limit solutions for $r \ll 1$ given by Eq. (7) and (8) are very good approximations to the exact GCM fits that have r = 0.29. When we additionally assume $\mu \gg 1$, the fast timescale prediction remains relatively accurate but the slow timescale reduces to 13 years and is hence underestimated by a factor of 2. We conclude that the $r \ll 1$ and $\mu \gg 1$ limit, Eq. (10) and (11), provide useful insight and have quantitative skill.

It is instructive to plot the evolution of T_1 and T_2 for the best fit solution (see Fig. 6 (b)). We also plot the globally-averaged SST and temperature at 120m depth from the MITgcm enabling the analytical solution to be compared to the GCM. Immediately after the eruption, the large temperature difference between the mixed layer and the deeper ocean results in large vertical heat exchange, with surface cooling being sequestered into the thermocline. In this first phase of relaxation, T_2 decreases and ocean heat exchange works in the same sense as climate feedbacks to damp the mixed layer response. The fast (order 1-year) timescale τ_f given by Eq. (7a) is controlled by $\lambda(1+\mu)$. Since $\mu = 2.3$, ocean damping is the dominant influence on the fast response. Held et al. (2010) and Gregory et al. (2016) note that the ocean plays a significant role on these short timescales but assume $\mu \leq 1$. As time proceeds, T_1 and T_2 approach one-another, and the system behaves like a single layer of thickness $h_1 + h_2$ relaxing on a much longer (20-year) timescale set by climate feedbacks. We see that sequestration of the temperature anomaly in to the interior ocean acts to temporarily shield it from surface damping, resulting in a lingering of the cold signal.

3.3 Time dependence of h_2 and q in response to a step forcing.

The subsurface ocean parameter values obtained by fitting the 2-box model to the MITgcm volcanic impulse responses ($q = 3.5$ Wm^{-2}K^{-1} and $h_2 = 150$m) stand in contrast to those reported in some previous studies (e.g. Geoffroy et al. 2013; Kostov et al. 2014) that investigated the response to step forcings of CO_2 in state-of-the-art GCMs (where $q \sim 1$ Wm^{-2}K^{-1} and $h_2 \sim 1000$m are found to be more typical). In Fig. 7, we explore the reasons behind the differences between an impulse and step response by simulating the response of the coupled MITgcm to a step forcing of -4 $Wm^{-2}K^{-1}$. This can be thought of as a 'perpetual volcanic eruption'. We compute h_2 and q as a function of time (from a best-fit line of the response), using the method outlined in Geoffroy et al. (2013, part I). Estimates are calculated over time periods spanning t = 0 to t_{max}, with t_{max} > 20 years, since the method only holds for $t >> \tau_f$. Other box model parameters are set to the values in Table 1. Fig. 7 (b) shows that q drops from ~3 to 1.1 $Wm^{-2}K^{-1}$ while h_2 increases from ~300 to 1015m over the 1000 years simulated. This time-dependency is associated with the temperature anomaly penetrating deeper into the ocean and activating process that act over longer periods of time. These deeper oceanic layers are associated with the ocean's meridional overturning circulation and are less likely to be fully excited by a short-lived Pinatubo-like eruption. Clearly, a study of the response of the climate to a single volcanic eruption can only address the short (year to decadal) rather than the long (centennial) timescales. Hence, the q parameter obtained from studies of a short-lived volcanic cooling are likely to differ from the ones relevant to the uptake of anthropogenic trace gases or CO_2 forcing. Indeed, the results from Romanou et al. (2017), who explored the uptake of CFCs, suggest a strong dependence of q with time, much as seen in Fig. 7 (b), because different components of the ocean circulation become activated as time progresses. Similarly, λ also changes in time in a manner that depends on regional feedbacks mediated by ocean heat transport (e.g. Armour et al. 2012). On the short (decadal) timescales relevant to volcanic responses, we find and believe that μ is large (perhaps ~3), with the subsurface ocean playing a significant role in the relaxation back towards equilibrium.

3.4 Climate sensitivity and the relative importance of atmospheric and oceanic damping

A number of studies (e.g. Lindzen & Giannitsis, 1998; Wigley et al. 2005; Yokohata et al. 2005; Hegerl et al. 2006; Bender et al. 2010; Merlis et al. 2014) have attempted to relate the response of SST following a volcanic eruption to some measure of the climate sensitivity. The methods used can be grouped as follows: (i) inferring ECS from the peak cooling in SST after an eruption (ii) inferring ECS from the integrated SST response and (iii) inferring transient climate sensitivity (TCS) from the integrated response. We now critically review these methods guided by our simulations and the simple models discussed in Section 3.2.

(i) Peak cooling and ECS

We begin our investigation by simulating idealized Pinatubo-like eruptions in the 2-box model for increasing values of λ, as shown in Fig. 8. All other parameters are kept constant and set to those in Table 1. In particular, since $\mu = 2.3$, oceanic processes play a very significant role in the evolution of the SST signal. We see that the peak cooling after the eruption decreases with increasing values of λ. Past studies (e.g. Wigley et al. 2005; Bender et al. 2010) have attempted to connect this peak cooling to λ (and hence the ECS), but did not find a strong link between the two quantities. While the effect of noise was invoked to explain this lack of correlation, we can use our 2-box model to explore further. By neglecting T_2 in Eq. (1) we can obtain an approximate expression for the peak cooling T_c after a pulse forcing that lasts a small but finite time Δt assumed to be about a year (details are given in the SI):

$$T_c \approx \frac{V}{\rho c_w h_1 + \frac{\lambda \Delta t(1+\mu)}{2}}, \qquad (13)$$

which reduces to Eq. (4) when Δt tends to zero. We see that when the forcing time is finite, the peak cooling T_c depends on both λ and q (through the parameter μ). In the limit of small μ, the ocean does not play a significant role and, in principle, the value of λ could be inferred from knowledge of V, T_c, Δt and h_1. However if $\mu \geq 1$, oceanic damping becomes as important as λ in reducing T_c and hence any correlation between the two can be confounded by the influence of ocean heat sequestration. Moreover, Fig. 8 shows that the influence of λ on the peak cooling is relatively small (especially for small Δt) and can easily be obscured by noise, as argued by Wigley et al. (2005), Bender et al. (2010) and Merlis et al. (2014).

(ii) Integrated response and ECS

To mitigate against the effect of noise, previous studies (e.g. Yokohata et al. 2005; Bender et al. 2010; Wigley et al. 2005) have attempted to link ECS to the time-integrated SST response, rather than just the peak cooling value. This approach can also be interpreted in terms of the 2-box model, by integrating Eq. (1) in time from t = 0 to ∞, giving:

$$\lambda \int_0^\infty \mathrm{T}_1(\mathrm{t})\mathrm{dt} = V. \tag{14}$$

Eq. (14) is a statement of conservation of energy: the energy extracted from the system by the volcanic eruption (RHS) must be balanced by the total energy recovered through climatic feedbacks (LHS) over the entire duration of the process. We note here parenthetically that since the time integrated response does not depend on ocean damping, the presence of an active deeper ocean underneath the mixed layer does not change the value of the integrated temperature response. A larger value of q tends to shift the weight of the response towards longer timescales, without affecting the 'area under the curve' (see Fig. 1).

The absence of the parameter q in Eq. (14) also means that the time integrated response can in theory be used to infer λ (or the ECS), without the conflating influence of ocean damping. A common problem, however, is that in complex GCMs and observations, the response typically becomes indistinguishable from noise 5-10 years after Pinatubo-like eruptions. If μ is small, the timescale of the response is dominated by the mixed layer and in that case, an integration time of 5-10 years may be enough to obtain a reliable estimate of λ. However if μ is large, a significant part of the cooling energy is stored in the subsurface ocean, and using Eq. (14) gives an overestimate of λ. For example, applying this method to our 2-box model fit with an integration time of 15 years gives $\lambda = 2.9$ $Wm^{-2}K^{-1}$, which is much larger than the value of 1.5 $Wm^{-2}K^{-1}$ obtained from our GCM's ECS. Moreover, Fig. 8 shows that the response curves (corresponding to different λ values) are tightly packed in the initial fast decay stage (0-3 years) but later become more distinct from each other. This overall behavior is reflective of the conclusion we drew from Eq. (10), that in the limit of large μ (and small r), the fast timescale is controlled by q, whereas the slower timescale is set by λ. Since in practice we are constrained to integrate over short periods of time due to noise, this further limits the usefulness of Eq. (14) for estimating the ECS.

It is likely that the sensitivity of the short-time evolution of SST to q, as well as λ, accounts for the large range of estimates of ECS inferred from volcanic eruptions that have been reported in the literature. Lindzen and Giannitsis (1998) simulated volcanic eruptions representing the ocean as a 1-D diffusion model to argue that a high ECS is not realistic, because it implies a much longer decay timescale than seen in observations. However, Wigley et al. (2005) argued that the slow decays simulated by Lindzen and Giannitsis (1998) were likely too long and find that an ECS as high as 4.5°C per doubling of CO_2 ($F_s = 3.7$ Wm^{-2}) cannot be discarded. Yokohata et al. (2005) rule out very high sensitivities (6.3°C) but find in their model that an ECS of 4.0°C produces results consistent with observations. For the same values of h_1, λ and diffusivity used by Lindzen and Giannitsis (1998) in a 1-D diffusion model (Appendix B), we obtain significantly shorter decay timescales than they reported. Our own results are more consistent with the timescales found by Santer et al. (2001) and Wigley et al. (2005).

(iii) Integrated response and TCS

Since the volcanic SST signal rapidly fades to noise for typical modern-era volcanic eruptions, Merlis et al. (2014) suggested that the SST response could provide a more reliable constraint on the transient climate sensitivity (TCS) instead of the long term ECS. The TCS is a measure of the response of the system while the deep ocean temperature has not been significantly affected by the forcing. This is perhaps a more relevant characterization of the evolution of the climate under anthropogenic CO_2 forcing than the ECS (e.g. Held et al. 2010). The TCS can be derived by setting $T_2 \ll T_1$ in Eq. (1):

$$\rho c_w h_1 \frac{dT_1}{dt} \approx -(\lambda + q)T_1 + F(t)\,, \tag{15}$$

yielding:

$$TCS = \frac{F_s}{\lambda + q}\,, \tag{16}$$

in the steady state, where $F(t) = F_s$.

The TCS is equivalent to the commonly used TCR, if F_s is the $2xCO_2$ forcing (e.g. Gregory & Forster, 2008). It is inversely proportional to the sum $\lambda + q$, as is the approximate fast timescale τ_f given in Eq. (7a). Held et al. (2010) and Gregory et al. (2016) employ the model given by Eq. (15) with λ and $q \sim 1\ Wm^{-2}K^{-1}$ and $h_1 \sim 100m$, which yields an impulse response with a single e-folding decay timescale of 5-10 years. While this is broadly in accord with typical volcanic response times, the approximation does not capture the two-timescale nature of the response, which is a very characteristic feature seen in our simulations. To reproduce the shape of the response with a fast (~ 1 year) and slow (~ 20 years) timescale, we require a 2-box model with a large value of q (~ 3.5 $Wm^{-2}K^{-1}$) and small value of h_2 (~ 150m). We cannot reproduce the 'dog-leg' shape with either a large value of h_2 (for any q) or a small value of q (for any h_2). We note that while the MITgcm may be over-emphasizing the ‘dog-leg’ in the response, it is also possible that natural fluctuations in SST could be obscuring the signal associated with the slower response timescale in other models. Our results, however, are consistent with the work of Wigley et al. (2005), who report a sharp (2-3 years) decay timescale after the eruption followed by a long ‘tail’ in the signal.

Merlis et al. (2014) propose to estimate the TCS by integrating Eq. (15) up to a time t_I short enough that $T_2 \ll T_1$, but long enough that the LHS of Eq. (15) becomes negligible. It is also assumed that the forcing has ceased to act before time t_I. The energy balance then becomes:

$$(\lambda + q) \int_0^{t_I} T_1(t) dt \approx V. \tag{17}$$

Eq. (17) states that the energy extracted by the forcing is approximately balanced by the energy dissipated by both atmospheric and oceanic damping up to time t_I (in contrast to Eq. (14) where the integral is carried to infinity). Merlis et al. (2014) use t_I = 15 years and find values of q that are on the order of 1 $Wm^{-2}K^{-1}$. However, using t_I = 15 years and applying this method to our 2-box model fit gives $\lambda + q = 2.9$ $Wm^{-2}K^{-1}$ and q = 1.4 $Wm^{-2}K^{-1}$. This is a large underestimate of the value that was found from curve fitting the MITgcm response (q = 3.5 $Wm^{-2}K^{-1}$). Based on Fig. 6 (b), we argue that an integration time of t_I = 15 years is too long to satisfy the condition $T_2 \ll T_1$. Beyond years 2-3, the deeper layer temperature anomaly (at around 120m depth) is of the same order of magnitude as the mixed layer temperature anomaly. When integrating with t_I = 3 years however, the LHS of Eq. (15) can no longer be neglected.

One way forward is to integrate Eq. (15) again, but this time take account of the transient term on the LHS to give:

$$(\lambda + q)\int_0^{t_I} T_1(t)dt \approx V - \rho c_w h_1 T_1(t_I). \quad (18)$$

Eq. (18) can be used to estimate λ + q more accurately than with Eq. (17), but requires knowledge of h_1 in addition to V and $T_1(t)$. Using Eq. (18) with t_I = 3 years, we find λ + q = 4.4 $Wm^{-2}K^{-1}$ and q = 2.9 $Wm^{-2}K^{-1}$. This is still an underestimate of the value of the curve fit value (q = 3.5 $Wm^{-2}K^{-1}$), but more accurate than the one obtained using Eq. (17) and t_I = 15 years. Further tests find that short integration times give better results than longer ones, despite still underestimating q. The method is also less accurate for large q values because this leads to a rapid increase in the magnitude of T_2, causing the approximation $T_2 \ll T_1$ to break down after only a short time. Nevertheless, using Eq. (18) and a short integration time could provide a way forward to estimate the TCS from knowledge of the SST response, h_1 and V. In practice, applying this method to observations would require averaging over a large number of eruptions, as the response can quickly be dominated by noise.

3.5 Accumulation potential

In Fig. 9, we use the 2-box model to assess the accumulation potential of the SST response from successive volcanic eruptions. We develop a metric for accumulation by considering a series of uniform eruptions spaced at a regular interval τ. Each eruption is modelled to extract one year's worth of energy from the system described by Eq. (1) and (2). As was seen in the aquaplanet simulations in Fig. 4, the peak magnitude of the response may increase over time if the response decay timescale is small relative to the interval between each eruption. We can obtain an analytical expression for the curve which passes through the peak temperature response following each eruption, which we term the envelope of the signal T_{en} (see SI for a detailed derivation):

$$T_{en}(t) = T_f \frac{1 - e^{-(t+\tau)/\tau_f}}{1 - e^{-\tau/\tau_f}} + T_s \frac{1 - e^{-(t+\tau)/\tau_s}}{1 - e^{-\tau/\tau_s}}. \tag{19}$$

In the limit that the repeated eruptions occur for all time ($t \rightarrow \infty$), the envelope asymptotes to a finite value T_∞ given by (see SI):

$$T_\infty = \frac{T_f}{1 - e^{-\tau/\tau_f}} + \frac{T_s}{1 - e^{-\tau/\tau_s}}. \tag{20}$$

This limit is reached when the rate at which cooling is supplied by the eruptions equals the rate at which it is lost through climate feedbacks. Eq. (20) thus provides a theoretical maximum cooling resulting from successive uniform eruptions. The analytical expression for T_∞ explicitly reveals how the potential for accumulation increases when the ratios τ/τ_f and τ/τ_s decrease. The first and second terms of Eq. (20) represent the contribution of the fast and the slow responses to the asymptotic peak temperature respectively. Since by definition τ_f is smaller than τ_s, the slow timescale contributes more to the signal accumulation than the fast one. For the parameter values in Table 1, we find that while the fast mode is negligibly enhanced, the slow mode grows over the slow timescale by a factor of 2.5 on moving from the initial to the equilibrium state. Moreover, we find that the cycle-average temperature at equilibrium is given by (see SI):

$$\bar{T}_\infty = \frac{V}{\lambda\tau}. \tag{21}$$

where V is the energy extracted by a volcanic eruption persisting for one year. It is useful to note that $\bar{T}_\infty$ tends to the ECS given by Eq. (12) when τ tends to 1 year and the forcing becomes essentially continuous.

In Fig. 9, we explore the sensitivity of the temperature envelope T_{en} to λ, q, h_1 and τ. The build-up amount is expressed relative to the peak cooling after the first eruption in the series, which varies with h_1, λ and q (see Eq. (13)). The blue points in each panel describe the accumulation curve obtained with the parameters from the 2-box fit to the MITgcm response (see Table 1). Fig. 9 (a) and (b) show that a smaller climate sensitivity λ and a larger mixed layer depth h_1 elicit a larger accumulation potential T_{en}. Both these parameters directly affect the relaxation of the mixed layer temperature and hence are of primary importance in setting the amount of accumulation. Fig. 9 (c) shows the effect of q in enhancing the accumulation potential T_{en}. A comparison with the aquaplanet results from Fig. 4 shows that the 2-box model (q = 3.5 $Wm^{-2}K^{-1}$) quantitatively captures the 20% increase in peak cooling seen in the full ocean configuration. Conversely, the 1-box model (q = 0) displays the same absence of accumulation as was observed in the slab configuration. Fig. 9 (d) shows the increase in response build-up as the interval between eruptions τ is narrowed. It shows that eruptions spaced by more than 20 years have a very low accumulation potential. Overall, the results of our analysis shows that for the range of parameters considered, a regular series of uniform eruptions can yield a maximum accumulation of approximately 10-50%. Moreover, ocean heat sequestration promotes accumulation, as indicated by the behavior of T_{en} with increasing q and h_1.

4. Response to the last millennium volcanic forcing

The role of the ocean in prolonging climate signals can be seen at work in the context of the volcanic forcing over the last millennium. A growing number of studies (e.g. Crowley, 2000; Hegerl et. al, 2003; Schurer et al. 2015; Atwood et al. 2016) have highlighted the importance of volcanic eruptions in instigating the coldest period of the Holocene, commonly referred to as the Little Ice Age (LIA, ~1250-1850 CE). They point to cooling induced by volcanoes as a major contributor to the LIA, beyond the effects of reduced insolation, changes in greenhouse gases, and land use evolution. Several authors (e.g. Free et al. 1999; Crowley et al. 2008; Stenchikov et al. 2009) have suggested that the ocean's long response timescales could help explain how eruptions that typically last only 1-2 years could engender cooling over multiple decades. Here, we make use of the MITgcm and the 2-box model to investigate the magnitude of the signal due to interaction with the ocean and the relative importance of small versus large eruptions.

Fig. 10 (adapted from Sigl et al. 2015) shows a reconstruction of Europe and Arctic temperatures along with global volcanic activity over the past 2000 years. The two panels show that 20 of the 40 coldest years in the series occurred during the Little Ice Age (LIA) and that those cold years often coincided with the largest eruptions of that period. The LIA was characterized by the occurrence of cold spells during the mid 15th, 17th and early 19th century. The spatial extent of the cooling is uncertain as proxy records originate largely from land in the Northern Hemisphere. Nevertheless, Neukom et al. (2014) suggest that sustained periods of cooling could also have occurred in the Southern hemisphere, particularly in the 17th century. Here, we focus on large tropical volcanic eruptions, because the stratospheric transport of particles toward the poles results in a considerable global impact (Robock, 2000). Moreover, the volcanic forcing reconstruction in Fig. 10 (a) indicates that tropical eruptions dominated over high latitude events over the past 2000 years.

Fig. 11 (a) shows an estimate of the volcanic forcing over the last millennium (A. LeGrande, personal communication). It is based on the reconstruction by Crowley and Unterman (2013) and represents the top-of-atmosphere shortwave flux anomaly in the GISS-E2-R model simulations. The forcing reveals the large volcanic eruptions of the 13th, 15th, 17th and 19th centuries as well as the smaller (> -4Wm^{-2}K^{-1}) eruptions that occurred more regularly throughout the timeseries. In Fig. 11 (b) and (c), we plot the MITgcm response of globally-averaged SSTs to this forcing, for the slab and full ocean configurations. These panels show that SSTs in the full ocean scenario tend to be colder than in the slab for the decades following clusters of large volcanic eruptions (13^{th}, 15^{th}, 17^{th} and 19^{th} centuries). Note that since the model does not contain ice, it does not capture the positive sea-ice feedback proposed by Miller et al. (2012) that link volcanism and the LIA. The differences in responses between the slab and full ocean configurations can be attributed to the sequestration of cold anomalies by the interior ocean.

Fig. 11 (c) shows that the strong volcanic activity of the 13^{th} century, which has previously been related to the onset of the LIA (e.g. Miller et al. 2012; Cole-Dai et al. 2013) has an effect that spans multiple decades. At the end of this sequence of eruptions, the temperature anomaly in the full ocean configuration remains mostly colder than the slab until the middle of the 15^{th} century. Similarly, after the large 1450's eruptions (Cole-Dai et al. 2013) the full ocean configuration displays a temperature anomaly of around -0.1°C that lasts for 100 years or so, in contrast to the slab, whose response decays to noise after only 20 years. There is also some signal prolongation after the 17^{th} century eruptions, which persists for around 20 years at the beginning of the 1800's. Finally, as reported by Crowley et al. (2008), the close packing of four eruptions between 1809 and 1835 (including the Tambora eruption in 1815) leads to an accumulated climate response in the 19^{th} century, because of the long timescales imparted by the global oceans.

Fig. 11 (d) shows the historical forcing responses of the box model obtained using the parameters in Table 1. Comparing Fig. 11 (b) and (d) shows that the box model reproduces the temperature anomalies of the MITgcm slab and full ocean configurations relatively well, indicating that the response remains mostly linear even on centennial timescales. However, as discussed in Section 2.2, very large eruptions in the MITgcm full ocean configuration induce some non-linearities due to increased mixed layer depths and a deeper sequestration of the cooling, particularly in the tropics. This causes a 10% decrease in the peak response relative to the linear case (approximately) but also a longer tail. The 2-box model does not capture this enhanced signal prolongation from large forcings, since it is calibrated to a Pinatubo-size eruption. Nevertheless, the 2-box model temperature is colder than the 1-box model temperature during 70% of the simulation, clearly highlighting the importance of the deeper ocean in extending the response. Fig. 11 (c) also shows the sensitivity of the box model to various values of the climate feedback λ, ranging from 0.8 to 2.5 $Wm^{-2}\,K^{-1}$. Small values of λ lead to longer prolongation as anticipated in Section 3, but without qualitative changes in the response.

In Fig. 11 (e), we use the 2-box model to estimate the contribution of the response from small eruptions ($>$ -4 Wm^{-2}) versus large eruptions ($\leq$ -4 Wm^{-2}). We find that small eruptions are frequent enough that their responses accumulate and cool the climate almost continuously throughout the entire timeseries by about 0.05°C. Large eruptions occur more rarely but can still lead to accumulation, e.g. 13th and 19th centuries. These results show that both small and large eruptions played an important part in the cooling of the climate during the last millennium. Moreover, the large volcanic eruptions from 1250 to 1850, coupled with the heat sequestration from the deeper ocean, could have been a significant driver of the extended periods of cooling observed during the LIA.

5. Discussion and conclusions

We have explored the role of the ocean in modulating the globally-averaged SST response of the climate to volcanic cooling, using a hierarchy of idealized models. We find that the presence of the deeper ocean beneath the mixed layer introduces a ‘dog-leg’ response characterized by two timescales. This effect strengthens with the parameter μ, which characterizes the ratio of ocean damping q and climatic feedback λ. In our study, curve-fitting the MITgcm response to a 2-box model gives $q = 3.5$ $Wm^{-2}K^{-1}$, $\lambda = 1.5$ $Wm^{-2}K^{-1}$ and $\mu = 2.3$. This value of μ leads to a pronounced 'dog-leg' in the response, with fast and slow timescales of 1 and 20 years respectively. In the limit of large μ, we find perhaps counter-intuitively, that the fast timescale is dominated by ocean damping, whereas the slow timescale is controlled by atmospheric feedbacks. Thus, in the first few years following the eruption, heat exchange with the subsurface ocean dominates over the climatic feedbacks in relaxing the SST response, sequestering the (negative) heat in to the ocean interior and reducing the magnitude of the peak anomaly. Subsequently, the cooling stored in the deeper ocean is delivered back to the surface over decadal periods, extending the response beyond the timescale implied by a slab ocean configuration.

For a forcing of the magnitude and duration of the Pinatubo eruption, we find that only the shallow (less than 200m) ocean plays a role in the response. This should be contrasted with the prolonged response involved in step CO_2 experiments which strongly 'activate' deeper components of the ocean circulation and its meridional overturning circulation (e.g. Kostov et al. 2013; Geoffroy et al. 2013 and Gregory et al. 2016). Hence, the q parameter obtained from studies of short-lived volcanic cooling will likely differ from the ones relevant to anthropogenic CO_2 forcing. To explore these connections, we simulated a step forcing of -4 Wm^{-2} in our coupled system and showed that the 2-box model parameters q and h_2 are strong functions of time. By employing the fitting method outlined in Geoffroy et al. 2013 (part I), we find that q decreases from ~ 3.5 $Wm^{-2}K^{-1}$ to 1.1 $Wm^{-2}K^{-1}$, while h_2 increases from $\sim$300 to 1015m over the 1000 years simulated. These results are consistent with Romanou et al.'s (2017) study of CFC uptake, who argue that q decreases strongly with time as different components of the ocean circulation become activated. This is analogous to the time-dependency of λ which is controlled by regional feedbacks mediated by ocean heat transport (e.g. Armour et al. 2012).

We went on to review methods that have been proposed for constraining climate sensitivity using the global-mean SST response to a volcanic eruption: (i) peak cooling, (ii) integrated response to estimate the ECS and (iii) integrated response to estimate the TCS. We find that natural variability masking the volcanic signal is a strong limiting factor in all such approaches. For methods (i) and (ii), we find that results can additionally be confounded by the effects of ocean heat uptake if $\mu > 1$. Moreover, we find that using method (iii) with short integration times can yield reasonable estimates for q, but the robustness of the approach declines with increasing μ. Since q is large in the immediate aftermath of an eruption, we argue that a study of the response of the climate to a single volcanic eruption can only address the short (year to decadal) rather than the longer (centennial) timescales involved in the response to step CO_2 forcings.

When $\mu > 1$, the resulting 'dog-leg' in the SST anomaly implies a longer prolongation of the response, which favors accumulation from successive eruptions. When forced by Pinatubo-like eruptions every 10 years, the peak temperature response grows by 20% over 100 years in the full ocean simulations, but does not grow in the slab ocean case. The accumulation behaves rather linearly in the GCM and can thus be represented by the 2-box model. We find that there is a limit to the theoretical maximum amount of accumulation that can occur for a series of regularly-spaced uniform eruptions, which decreases with the climatic feedback λ and increases with the mixed layer depth h_1. For typical parameter values, this maximum accumulation potential is around 10-50% of the initial peak cooling. We also note that the accumulation rate decreases sharply when the interval between eruptions becomes larger than the slow decay timescale (20 years).

Finally, we demonstrate how signal prolongation and accumulation due to the presence of the subsurface ocean reservoir could help explain the extended periods of cooling observed during the Little Ice Age (LIA, ~1250-1850 CE). After the large clusters of eruptions of the 13^{th}, 15^{th}, 17^{th} and 19^{th} century, the subsurface ocean prolongs the surface cooling over multiple decades. In particular, after the large eruptions of the 1450's, we find a globally-averaged SST anomaly of -0.1°C that lasts for 100 with an active ocean versus 20 years with a slab ocean. When calibrated to a Pinatubo-like forcing, the 2-box model provides a reasonable representation of the MITgcm historical response, but tends to underestimate the signal prolongation after much larger eruptions because it does not capture the deepest sequestration of cold anomalies. The box model reveals that frequent small scale eruptions tended to cool the climate almost continuously by about -0.05°C throughout the last millennium. Larger eruptions were rarer, but aided by ocean heat sequestration, could have played an important part in extended periods of cooling during the LIA. These results are in line with the conclusions from Crowley et al. (2008), Miller et al. (2012), Cole-Dai et al. (2013), Atwood et al. (2016) and others. We thereby conclude that the mechanisms responsible for storing volcanic cooling in the subsurface ocean are relevant for questions pertaining to climatic cooling over decadal to centennial timescales.

Acknowledgements

MG acknowledges support from the John H. Carlson fellowship and JM from the NSF FESD Ozone project. We would like to thank Allegra Legrande from NASA GISS for her support in this work and for the data on volcanic forcing during the last millennium. We are also most grateful for informative discussions with Susan Solomon, Jean-Michel Campin, Brian Green and Paul O'Gorman.

Appendix A: MITgcm coupled model

This study employs the Massachusetts Institute of Technology Global Circulation Model (MITgcm; Marshall et al. 1997a,b) in a coupled atmosphere-ocean configuration. The atmosphere and ocean fluids both use the same C32 cubed-sphere grid (32×32 cells per face), yielding a nominal horizontal resolution of 2.8° (Adcroft et al. 2004; Adcroft and Campin 2004). The ocean is uniformly 3.4 km deep and has 15 vertical levels with grid spacing increasing from 30 m at the surface to 400 m at depth. Effects of mesoscale eddies are parameterized as an advective process (Gent & McWilliams, 1989) and isopycnal diffusion (Redi, 1982). Convective adjustment is implemented as an enhanced vertical mixing of temperature and salinity and is used to represent ocean convection (Klinger and Marshall 1995). The background vertical diffusion is uniform and set to 3×10^{-5} m^2s^{-1}.

The atmospheric component of the model has 26 pressure levels and employs a gray radiation scheme with parameterized convection and precipitation as in Frierson et al. (2006).The longwave optical thickness is modified by the distribution of water vapor, following Byrne & O'Gorman (2012). In this simplified radiation scheme, the shortwave flux does not interact with the atmosphere and hence the planetary albedo is the same as the surface albedo. There are no clouds in the model. A seasonal cycle of insolation at the top of the atmosphere is specified for a solar constant of 1360 Wm^{-2}. The meridional albedo contrast is represented by a pole-to-equator albedo gradient varying linearly from 0.6 to 0.2 (see Fig. A1), in line with the observations presented in Donohoe and Battisti (2011).

We also make use of a ‘slab ocean’ configuration of the MITgcm that has a single layer in the vertical, whose thickness is fixed in time but varies spatially according to the annual-mean mixed layer depth diagnosed from a long control simulation according to the method outlined in Kara et al. (2000). Surface heat fluxes are imposed as a stationary boundary condition to the slab ocean model. These heat fluxes are also diagnosed from the control simulation and represent ocean energy transport convergence into a given grid box.

Appendix B: The 1-D diffusion model

1-D diffusion models such as the one presented in Fig. A2 have been employed in previous studies to represent processes occurring in the global ocean (e.g. Lindzen & Giannitsis, 1998). The model considered here consists of a mixed layer of uniform temperature T_1 and depth h_1 above a diffusive layer of finite depth H with temperature T(z). The mixed layer is forced from the top by a forcing F and damped by climate feedbacks λT_1. In the diffusive layer, the thermal diffusivity is κ. For consistency with the rest of the analysis, the mixed layer depth and climate sensitivity parameter are fixed to the following values: $h_1 = 43$m and $\lambda = 1.5$ $Wm^{-2}K^{-1}$. The depth H is chosen to be 1000m, deep enough for the temperature anomalies after a volcanic eruption to be negligible. The model satisfies:

$$\rho c_w h_1 \frac{dT_1(t)}{dt} = F(t) - \lambda T_1(t) - \rho c_w \kappa \frac{\partial T(z=-h_1,t)}{\partial z} \qquad \text{(A9)}$$

and

$$\frac{\partial T(z,t)}{\partial t} = \frac{\partial}{\partial z}\left(\kappa \frac{\partial T(z,t)}{\partial z}\right) \qquad \text{(A10)}$$

with boundary conditions:

$$T(z=0,t) = T_1(t) \qquad \text{(A11)}$$

and

$$\frac{\partial T(z=-H,t)}{\partial z} = 0 \qquad \text{(A12)}$$

This set of equations are solved numerically with second-order accuracy in space and a backward first-order difference in time. Fig. A3 shows that the 1-D diffusion model provides a relatively good fit to the full ocean MITgcm configuration for $\kappa = 10^{-4}$ m^2s^{-1}, but does not capture the ‘dog-leg’ shape as well as the 2-box model. The 1-D model solution tends to the slab solution as the diffusivity becomes very small ($\kappa = 10^{-7}$ m^2s^{-1}). In the presence of an active deeper ocean, the diffusion model reproduces the reduced peak cooling and the prolonged response that was observed in the 2-box model and in the MITgcm full ocean configuration.

Fig. A4 shows that after 3 years, the diffusion model and the MITgcm have a similar temperature evolution with depth. The magnitude of the temperature anomaly decreases with time over the top layers of the ocean and increases in the layers underneath through the combined action of the climatic feedbacks at the surface and the ocean exchanges drawing cold temperatures into the ocean depth.

References

Adcroft, A., Campin, J.-M., Hill, C., & Marshall, J. (2004). Implementation of an Atmosphere–Ocean General Circulation Model on the Expanded Spherical Cube. Monthly Weather Review, 132(1996), 2845–2863. doi:10.1175/MWR2823.1.

Adcroft, A., & Campin, J. M. (2004). Rescaled height coordinates for accurate representation of free-surface flows in ocean circulation models. Ocean Modelling, 7(3–4), 269–284. doi:10.1016/j.ocemod.2003.09.003

Armour, K. C., Bitz, C. M., & Roe, G. H. (2013). Time-varying climate sensitivity from regional feedbacks. Journal of Climate, 26(13), 4518-4534. doi:10.1175/JCLI-D-12-00544.1

Atwood, A. R., Wu, E., Frierson, D. M. W., Battisti, D. S., & Sachs, J. P. (2016). Quantifying climate forcings and feedbacks over the last millennium in the CMIP5/PMIP3 models. Journal of Climate.

Bender, F. A. M., Ekman, A. M., & Rodhe, H. (2010). Response to the eruption of Mount Pinatubo in relation to climate sensitivity in the CMIP3 models. Climate dynamics, 35(5), 875-886.

Byrne, M. P., & Gorman, P. A. (2012). Land – Ocean Warming Contrast over a Wide Range of Climates : Convective Quasi-Equilibrium Theory and Idealized Simulations. Journal of Climate, 26, 4000–4016. http://doi.org/10.1175/JCLI-D-12-00262.1

Church, J. A., White, N. J., & Arblaster, J. M. (2005). Significant decadal-scale impact of volcanic eruptions on sea level and ocean heat content. Nature, 438(7064), 74-77.

Cole-Dai, J., Ferris, D. G., Lanciki, A. L., Savarino, J., Thiemens, M. H., & McConnell, J. R. (2013). Two likely stratospheric volcanic eruptions in the 1450s CE found in a bipolar, subannually dated 800 year ice core record. Journal of Geophysical Research: Atmospheres, 118(14), 7459-7466.

Crowley, T. J. (2000). Causes of Climate Change Over the Past 1000 Years. Science, 270. http://doi.org/10.1126/science.289.5477.270

Crowley, T. J., Zielinski, G., Vinther, B., Udisti, R., Kreutz, K., Cole-Dai, J., & Castellano, E. (2008). Volcanism and the little ice age. PAGES news, 16(2), 22-23.

Crowley, T. J., & Unterman, M. B. (2013). Technical details concerning development of a 1200 yr proxy index for global volcanism. Earth System Science Data, 5(1), 187-197.

Donohoe, A., & Battisti, D. (2011). Atmospheric and Surface Contributions to Planetary Albedo. Journal of Climate, 24, 4402–4418. http://doi.org/10.1175/2011JCLI3946.1

Ferreira, D., Marshall, J., & Campin, J.-M. (2009). Localization of Deep Water Formation : Role of Atmospheric Moisture Transport and Geometrical Constraints on Ocean Circulation. Journal of Climate, 23, 1456–1476. http://doi.org/10.1175/2009JCLI3197.1

Free, M., & Robock, A. (1999). Global warming in the context of the Little Ice Age. Journal of Geophysical Research: Atmospheres, 104(D16), 19057-19070.

Frierson, D. M. W., Held, I. M., & Zurita-Gotor, P. (2006). A Gray-Radiation Aquaplanet Moist GCM. Part I : Static Stability and Eddy Scale. Journal of the Atmospheric Sciences, 63, 2548–2566.

Gent, P., & McWilliams, J. (1989). Isopycnal mixing in ocean circulation models. Journal of Physical Oceanography, 20.

Geoffroy, O., Saint-Martin, D., Bellon, G., Voldoire, A., Olivié, D. J. L., & Tytéca, S. (2013). Transient climate response in a two-layer energy-balance model. Part I: Analytical Solution and Parameter Calibration Using CMIP5 AOGCM Experiments . Journal of Climate, 26, 1841–1857. http://doi.org/10.1175/JCLI-D-12-00196.1

Gleckler, P. J., Wigley, T. M. L., Santer, B. D., Gregory, J. M., AchutaRao, K., & Taylor, K. E. (2006). Volcanoes and climate: Krakatoa's signature persists in the ocean. Nature, 439(7077), 675-675.

Green, B., & Marshall, J. (2017). Coupling of Trade Winds with Ocean Circulation Damps ITCZ Shifts. Journal of Climate, 30(12), 4395-4411.

Gregory, J. M. (2000). Vertical heat transports in the ocean and their effect on time-dependent climate change. Climate Dynamics, 16, 501–515. http://doi.org/10.1007/s003820000059

Gregory, J. M., & Forster, P. M. (2008). Transient climate response estimated from radiative forcing and observed temperature change. Journal of Geophysical Research: Atmospheres, 113(D23).

Gregory, J. M., Andrews, T., Good, P., Mauritsen, T., & Forster, P. M. (2016). Small global-mean cooling due to volcanic radiative forcing. Climate Dynamics, 47(12), 3979-3991.

Hansen, J., Russell, G., Lacis, A., Fung, I., Rind, D., & Stone, P. (1985). Climate response times: dependence on climate sensitivity and ocean mixing. Science, 229, 857-860.

Hegerl, G. C., Crowley, T. J., Baum, S. K., Kim, K., & Hyde, W. T. (2003). Detection of volcanic , solar and greenhouse gas signals in paleo-reconstructions of Northern Hemispheric temperature. Geophysical Research Letters, 30, 94–97. http://doi.org/10.1029/2002GL016635

Held, I. M., Winton, M., Takahashi, K., Delworth, T., Zeng, F., & Vallis, G. K. (2010). Probing the Fast and Slow Components of Global Warming by Returning Abruptly to Preindustrial Forcing. Journal of Climate, 23(9), 2418–2427. http://doi.org/10.1175/2009JCLI3466.1

Kara, A. B., Rochford, P. A., & Hurlburt, H. E. (2000). An optimal definition for ocean mixed layer depth. Journal of Geophysical Research: Oceans, 105(C7), 16803-16821.

Klinger, B. A., & Marshall, J. (1995). Regimes and scaling laws for rotating deep convection in the ocean. Dynamics of Atmospheres and Oceans, 21, 227–256.

Kostov, Y., Armour, K., & Marshall, J. (2013). Impact of the Atlantic Meridional Overturning Circulation on Ocean Heat Storage and Transient Climate Change. Geophysical Research Letters, 1–9. http://doi.org/10.1002/2013GL058998.1.

Lebedeff, S. A. (1988). Analytic solution of the box diffusion model for a global ocean. Journal of Geophysical Research, 93.

Lindzen, R. S., & Giannitsis, C. (1998). On the climatic implications of volcanic cooling. Journal of Geophysical Research, 103, 5929–5941. http://doi.org/10.1029/98JD00125

Marshall, J., Adcroft, A., Hill, C., Perelman, L., & Heisey, C. (1997). A finite-volume, incompressible Navier Stokes model for studies of the ocean on parallel computers. Journal of Geophysical Research, 102, 5753–5766.

Marshall, J., Hill, C., Perelman, L., & Adcroft, A. (1997). Hydrostatic, quasi-hydrostatic, and non hydrostatic ocean modelling. Journal of Geophysical Research, 102, 5733–5752.

Merlis, T. M., Held, I. M., Stenchikov, G. L., Zeng, F., & Horowitz, L. W. (2014). Constraining transient climate sensitivity using coupled climate model simulations of volcanic eruptions. Journal of Climate, 27(20), 7781–7795. http://doi.org/10.1175/JCLI-D-14-00214.1

Mignot, J., Khodri, M., Frankignoul, C., & Servonnat, J. (2011). Volcanic impact on the Atlantic Ocean over the last millennium. Climate of the Past Discussions, 7, 2511-2554.

Miller, G. H., Geirsdóttir, Á., Zhong, Y., Larsen, D. J., Otto-bliesner, B. L., Holland, M. M., … Björnsson, H. (2012). Abrupt onset of the Little Ice Age triggered by volcanism and sustained by sea-ice/ocean feedbacks. Geophysical Research Letters, 39, 1–5. http://doi.org/10.1029/2011GL050168

Neukom, R., Gergis, J., Karoly, D. J., Wanner, H., Curran, M., Elbert, J., … Mundo, I. (2014). Inter-hemispheric temperature variability over the past millennium. Nature Climate Change, 4. http://doi.org/10.1038/NCLIMATE2174

Otterå, O. H., Bentsen, M., Drange, H., & Suo, L. (2010). External forcing as a metronome for Atlantic multidecadal variability. Nature Geoscience, 3(10), 688.

Redi, M. (1982). Oceanic isopycnal mixing. Journal of Physical Oceanography, 12.

Robock, A. (2000). Volcanic eruptions and climate. Reviews of Geophysics, 38(2), 191–219. http://doi.org/10.1029/1998RG000054

Romanou, A., et al. "Role of the Ocean's AMOC in setting the Uptake Efficiency of Transient Tracers." Geophysical Research Letters.

Santer, B. D., Wigley, T. M. L., Doutriaux, C., Boyle, J. S., Hansen, J. E., Jones, P. D., ... & Taylor, K. E. (2001). Accounting for the effects of volcanoes and ENSO in comparisons of modeled and observed temperature trends. Journal of Geophysical Research: Atmospheres, 106(D22), 28033-28059

Schurer, A. P., Hegerl, G. C., & Obrochta, S. P. (2015). Determining the likelihood of pauses and surges in global warming. Geophysical Research Letters, 42(14), 5974-5982.

Sigl, M., Winstrup, M., McConnell, J. R., Welten, K. C., Plunkett, G., Ludlow, F., … Woodruff, T. E. (2015). Timing and climate forcing of volcanic eruptions for the past 2,500 years. Nature, 523(7562), 543–549. http://doi.org/10.1038/nature14565

Soden, B. J., Wetherald, R. T., Stenchikov, G. L., & Robock, A. (2000). Global Cooling After the Eruption of Mount Pinatubo : A Test of Climate Feedback by Water Vapor. Science, 296.

Stenchikov, G., Delworth, T. L., Ramaswamy, V., Stouffer, R. J., Wittenberg, A., & Zeng, F. (2009). Volcanic signals in oceans, 114, 1–13. http://doi.org/10.1029/2008JD011673

Stouffer, R. J. (2004). Time scales of climate response. Journal of Climate, 17(1), 209-217.

Tsutsui, J., 2017: Quantification of temperature response to CO_2 forcing in atmosphere-ocean general circulation models. Climatic Change, 140, 287-305.

Wigley, T. M. L., Ammann, C. M., Santer, B. D., & Raper, S. C. (2005). Effect of climate sensitivity on the response to volcanic forcing. Journal of Geophysical Research: Atmospheres, 110(D9).

Winton, M., Takahashi, K., & Held, I. M. (2010). Importance of Ocean Heat Uptake Efficacy to Transient Climate Change. Journal of Climate, 23, 2333–2344. http://doi.org/10.1175/2009JCLI3139.1

Yokohata, T., Emori, S., Nozawa, T., Tsushima, Y., Ogura, T., & Kimoto, M. (2005). Climate response to volcanic forcing: Validation of climate sensitivity of a coupled atmosphere-ocean general circulation model. Geophysical Research Letters, 32(21).

Figure caption list

Fig. 1: Response of the box model to an idealized Pinatubo eruption (-4 W/m^2 for a year) in the 1-box case (red) and 2-box cases (blue) plotted for several values of the ratio $\mu = q/\lambda$, where λ is the climatic feedback parameter, here kept constant at $\lambda = 1.5 Wm^{-2}K^{-1}$ and q is a measure of the ocean heat uptake. The ‘area under the curve’ is the same in all cases, but with a smaller peak and a longer ‘tail’ as q (or μ) increases.

Fig. 2: MITgcm responses to a Pinatubo-like forcing (-4 Wm^{-2} for a year) and a 10×Pinatubo forcing (-40 Wm^{-2} for a year) for the slab ocean in red and the full ocean configuration in blue. (a) Ensemble mean responses normalized with respect to their maximum cooling temperature. (b) Non-normalized responses for the Pinatubo forcing with the shaded envelopes of 5 ensemble members for the slab ocean (red) and 10 ensemble members for the full ocean (blue). The solid lines are the corresponding ensemble mean. (c) Non-normalized responses for the 10×Pinatubo forcing with one ensemble member for the slab and full ocean respectively.

Fig. 3: MITgcm zonally averaged temperature anomaly in the ocean with depth and latitude in the full ocean configuration. The temperature evolution is shown for 2, 5 and 10 years after the eruption in the left, middle and right panels respectively. The top panels are the mean responses of 10 ensemble members for the Pinatubo-like forcing (-4 Wm^{-2} for a year). The bottom panels are the responses for a single ensemble member of the 10×Pinatubo forcing (-40 Wm^{-2} for a year). The thick black line represents the model-diagnosed zonally-averaged mixed layer depth.

Fig. 4: MITgcm ensemble-mean response to a Pinatubo-like eruption (-4 Wm^{-2} for 1 year) every 10 years in the slab ocean (red) and full ocean (blue) configurations. The slab and full ocean configuration were run for 5 and 10 ensemble members respectively.

Fig. 5: 2-box model comprising a mixed layer of depth h_1 and a deeper ocean of depth h_2 with temperature anomalies T_1 and T_2 respectively. The model is driven from the top by an external forcing F and damped by the climate feedback λT_1. The two boxes exchange heat through the exchange parameter q.

Fig. 6: Temperature responses of the box model (solid lines) and the MITgcm (dotted lines) to an idealized Pinatubo forcing (-4 Wm^{-2} for a year). (a) 2-box model fit (solid blue) to the full ocean MITgcm response (dotted blue) with $r^2 = 0.87$ and 1-box model fit (solid red) to the slab ocean MITgcm response (dotted red) with $r^2 = 0.97$. The fitted parameters are summarized in Table 1. (b) SST (dotted blue) and temperature at 120m depth (dotted orange) from the MITgcm full ocean configuration with the corresponding 2-box model temperatures T_1 (solid blue) and T_2 (solid orange).

Fig. 7: (a) Response of the MITgcm full ocean to a step forcing of -4 Wm^{-2} in blue and best-fit response with fitting accuracy $R^2 = 0.89$ in black. (b) Time-dependency of q (blue) and h_2 (orange) during the step response evaluated using the method of Geoffroy et al. (2013, part I) over the best-fit line (see text).

Fig. 8: 2-box model responses to an idealized Pinatubo forcing (-4 Wm^{-2} for a year) for a range of λ (or ECS) values. All other parameters are fixed to those in Table 1.

Fig. 9: Normalized temperature envelope T_{en} for a series of uniform and regularly spaced eruptions in the 2-box model. Each dot represents the peak cooling temperature after a new eruption. Parameter sensitivity is explored for (a) the climate sensitivity λ, (b) the mixed layer depth h_1, (c) the ocean exchange parameter q and (d) the time interval between eruptions τ.

Fig. 10: (a) 2000-year reconstruction of global volcanic aerosol forcing from sulfate composite records from tropical (orange) and Northern Hemisphere (gray) eruptions. (b) 2000-year record of reconstructed summer temperature anomalies for Europe and the Arctic relative to 1961-1990 shown yearly (green) and as a 50-year running mean (orange). The 40 coldest single years are indicated with blue circles and the approximate duration of the Little Ice Age is shown. Data taken from Sigl et al. (2015).

Fig. 11: (a) Tropical volcanic forcing of the last millennium (A. LeGrande, NASA GISS, personal communication) divided into small (> -4 Wm^{-2}) and large eruptions (≤ -4 Wm^{-2}). (b) responses of the MITgcm coupled model with a full ocean (blue) and a slab ocean (red) to the volcanic forcing shown in (a). (c) 5-year running mean of (b) on a magnified scale. (d) Reconstructed response obtained by convolving the forcing in (a) with the response functions (red and blue) shown in Fig. 6 (a) and sensitivity to λ (shading). (e) 5-year running mean of the 2-box model response to the small (black) and large (gray) volcanic forcing.

Fig. A1. Linear albedo gradient imposed at the surface of the MITgcm model. The grid is in a cubed sphere configuration with 32×32 points per face, with a nominal horizontal resolution of 2.8°. The thick black lines indicate the solid ridges of the ‘double-drake’ setup extending from the North Pole to 35°S and set 90° apart.

Fig. A2: 1-D diffusion model with mixed layer depth h_1, deep ocean depth H, thermal diffusivity κ, climate feedback parameter λ, mixed layer temperature T_1 and deep ocean temperature T(z).

Fig. A3: Mixed layer temperature anomaly in the 1-D diffusion model (solid lines) and MITgcm (dotted lines) for a -40 Wm^{-2}K pulse lasting 1 year. The red lines correspond to a slab ocean whereas the blue lines are for a full ocean. The response functions are shown for (a) non-normalized values and (b) normalized by the corresponding peak cooling value.

Fig. A4: Time evolution of temperature profiles with depth for a 1-year forcing of -40 Wm^{-2} in (a) the 1-D diffusion model with $\kappa = 10^{-4}\ m^2s^{-1}$ and (b) the horizontally MITgcm full ocean configuration.

Parameter	**Physical interpretation**	**Exact fit**	**Approximation ($r \ll 1$)**	**Approximation ($r \ll 1, \mu \gg 1$)**
h_1	Mixed layer depth	43 m	43 m	43 m
h_2	Deeper ocean depth	150 m	150 m	150 m
λ	Climatic feedback	1.5 $Wm^{-2}K^{-1}$	1.5 $Wm^{-2}K^{-1}$	1.5 $Wm^{-2}K^{-1}$
q	Oceanic mixing	3.5 $Wm^{-2}K^{-1}$	3.5 $Wm^{-2}K^{-1}$	3.5 $Wm^{-2}K^{-1}$
μ	Ratio of ocean to climatic damping (q/λ)	2.3	2.3	2.3
r	Heat capacity ratio (h_1/h_2)	0.29	0.29	0.29
τ_f	Fast timescale	1.0 years	1.2 years	1.6 years
τ_s	Slow timescale	22.0 years	19.2 years	13.4 years
T_f/T_c	Fast amplitude	0.86	0.88	0.78
T_s/T_c	Slow amplitude	0.14	0.12	0.22

Table 1: 2-box model parameters obtained by curve-fitting the SST response of the full ocean MITgcm to an idealized Pinatubo eruption (-4 W/m^2 for a year).

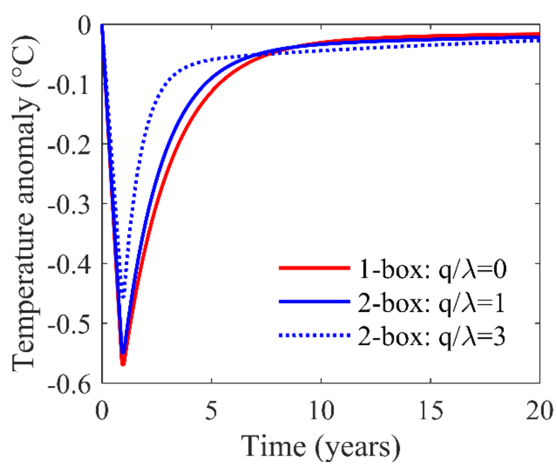

Fig. 1: Responses of the box model to an idealized Pinatubo eruption (-4 W/m^2 for a year) in the 1-box case (red) and 2-box cases (blue) in terms of the ratio of ocean mixing strength to the climatic feedback parameter $\mu = q/\lambda$ with $\lambda = 1.5 Wm^{-2}K^{-1}$. The 'area under the curve' is the same in all cases, but with a smaller peak and a longer 'tail' as q (or μ) increases.

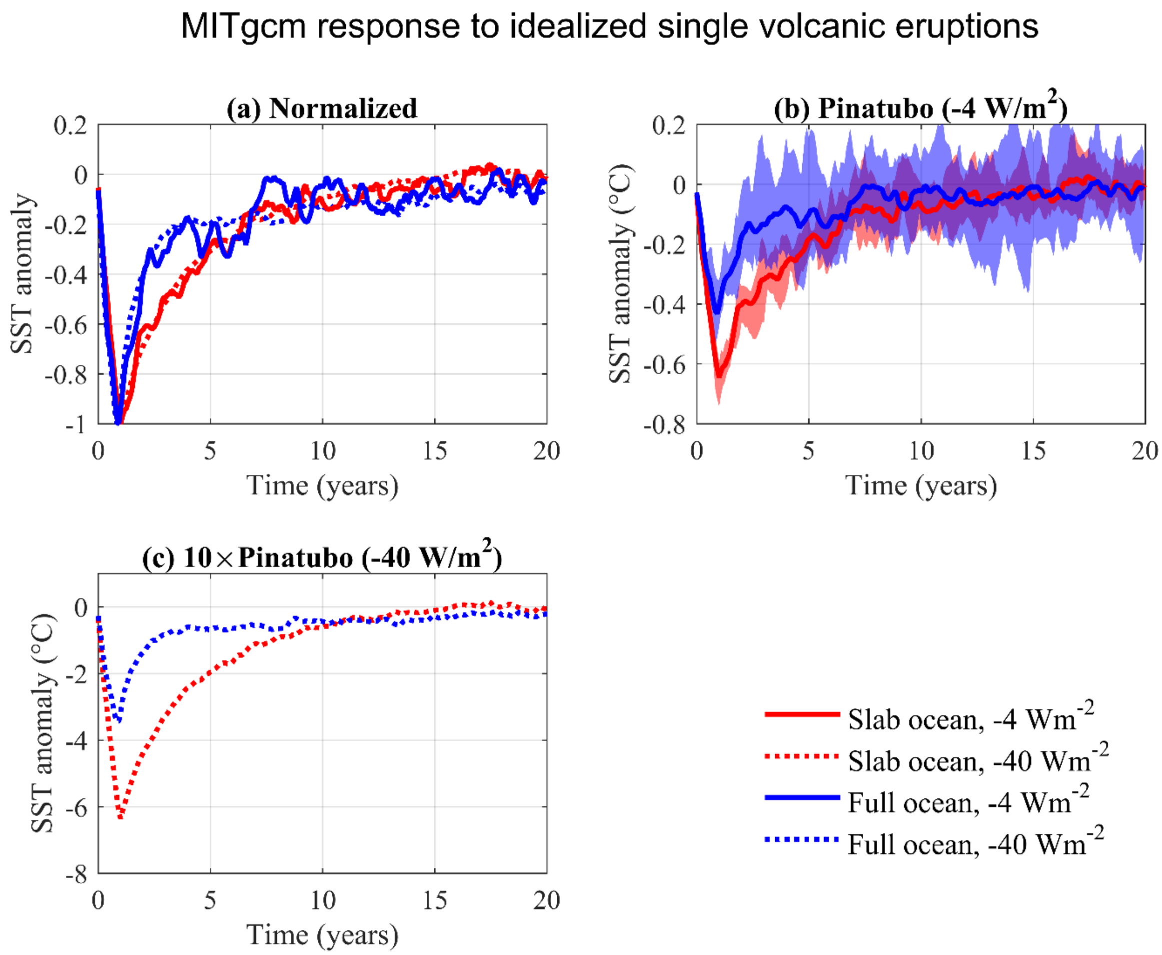

Fig. 2: MITgcm responses to a Pinatubo-like forcing (-4 Wm^{-2} for a year) and a 10×Pinatubo forcing (-40 Wm^{-2} for a year) for the slab ocean in red and the full ocean configuration in blue. (a) Ensemble mean responses normalized with respect to their maximum cooling temperature. (b) Non-normalized responses for the Pinatubo forcing with the shaded envelopes of 5 ensemble members for the slab ocean (red) and 10 ensemble members for the full ocean (blue). The solid

lines are the corresponding ensemble mean. (c) Non-normalized responses for the 10×Pinatubo forcing with one ensemble member for the slab and full ocean respectively.

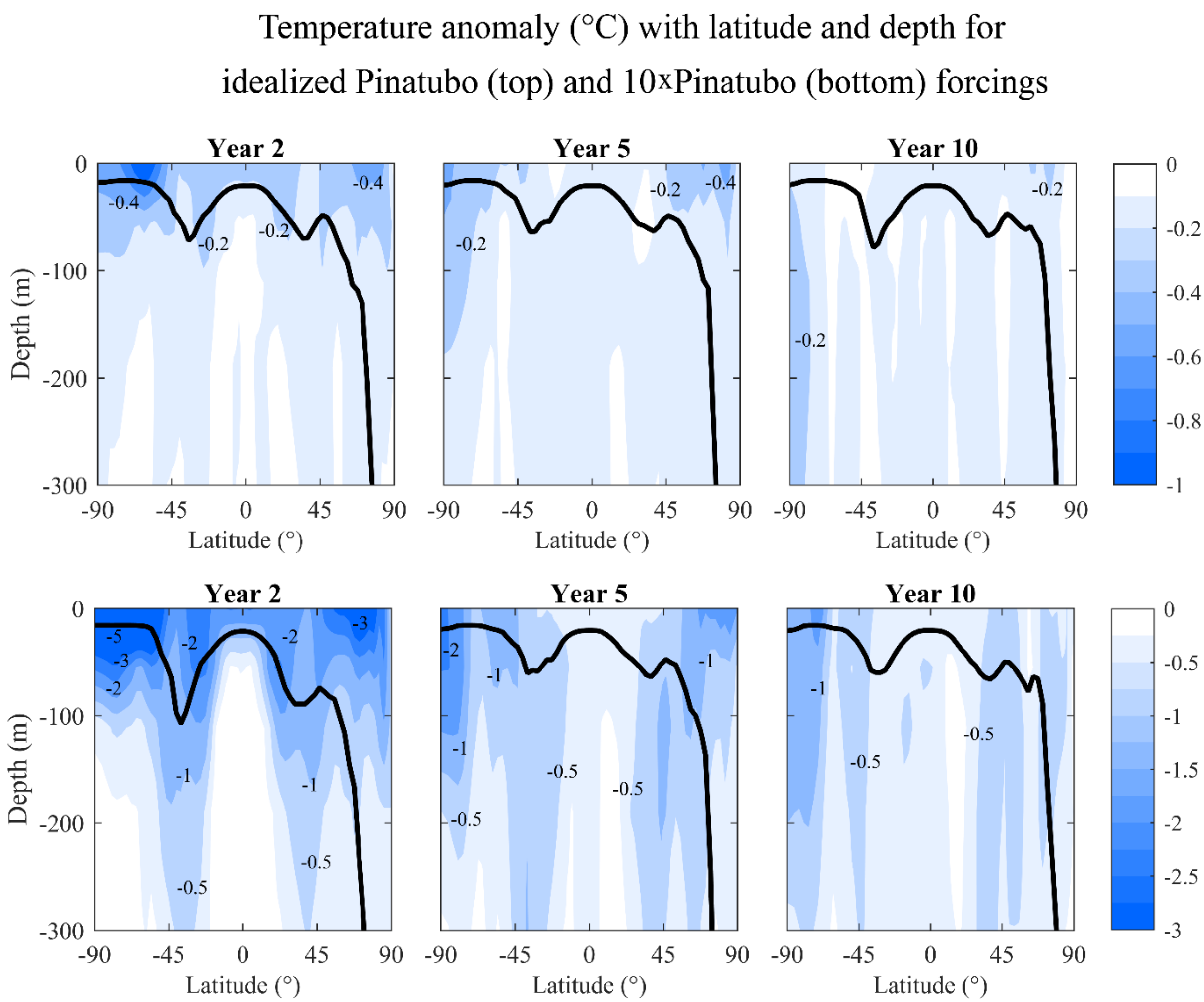

Fig. 3: MITgcm zonally averaged temperature anomaly in the ocean with depth and latitude in the full ocean configuration. The temperature evolution is shown for 2, 5 and 10 years after the eruption initiation in the left, middle and right panels respectively. The top panels are the mean responses of 10 ensemble members for the Pinatubo-like forcing (-4 Wm^{-2} for a year) and the bottom panels are the responses for a single ensemble member of the 10×Pinatubo forcing (-40 Wm^{-2} for a year). The thick black line represents the model-diagnosed zonally-averaged mixed layer depth.

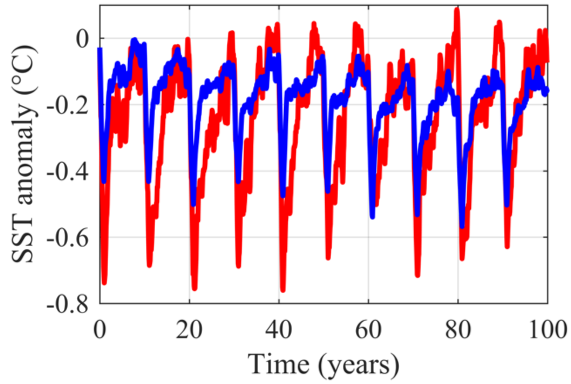

Fig. 4: MITgcm ensemble-mean response to a Pinatubo-like eruption (-4 Wm^{-2} for a year) every 10 years in the slab ocean (red) and full ocean (blue) configurations. The slab and full ocean configuration were run for 5 and 10 ensemble members respectively.

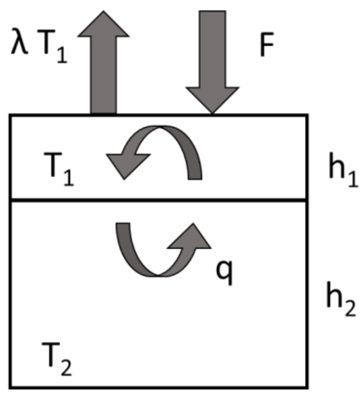

Fig. 5: 2-box model comprising a mixed layer of depth h_1 and a deeper ocean of depth h_2 with temperature anomalies T_1 and T_2 respectively. The model is driven from the top by an external forcing F and damped by the climate feedback λT_1. The two boxes exchange heat through the exchange parameter q.

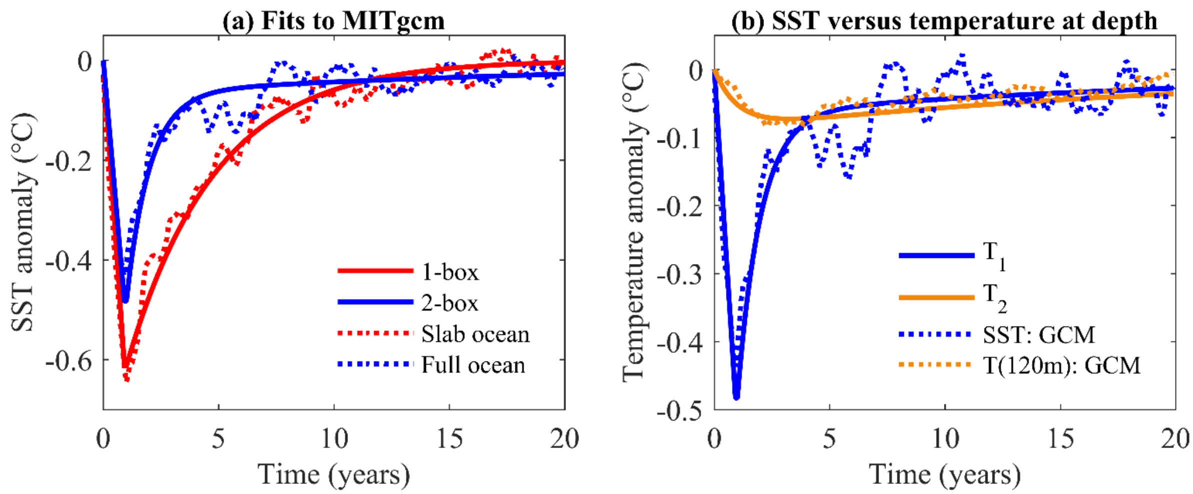

Fig. 6: Temperature responses of the box model (solid lines) and the MITgcm (dotted lines) to an idealized Pinatubo forcing (-4 Wm^{-2} for a year). (a) 2-box model fit (solid blue) to the full ocean MITgcm response (dotted blue) with a fitting accuracy $R^2 = 0.87$ and 1-box model fit (solid red) to the slab ocean MITgcm response (dotted red) with $R^2 = 0.97$. The fit parameters are summarized in Table 1. (b) SST (dotted blue) and temperature at 120m depth (dotted orange) from the MITgcm full ocean configuration with the corresponding 2-box model temperatures T_1 (solid blue) and T_2 (solid orange).

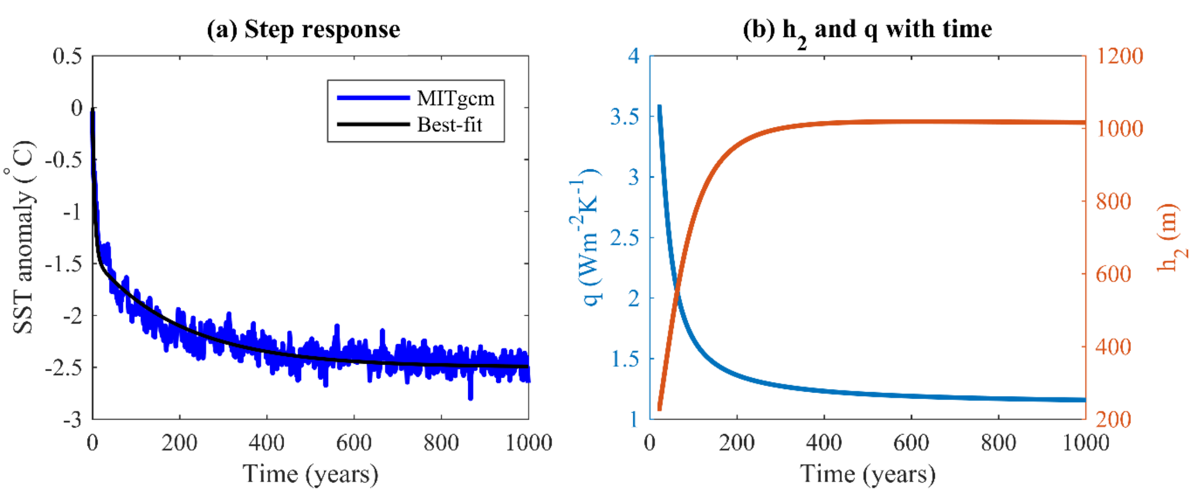

Fig. 7: (a) Response of the MITgcm full ocean to a step forcing of -4 Wm^{-2} in blue and best-fit response with fitting accuracy $R^2 = 0.89$ in black. (b) Time-dependency of q (blue) and h_2 (orange) during the step response evaluated using the method of Geoffroy et al. (2013, part I) over the best-fit line (see text).

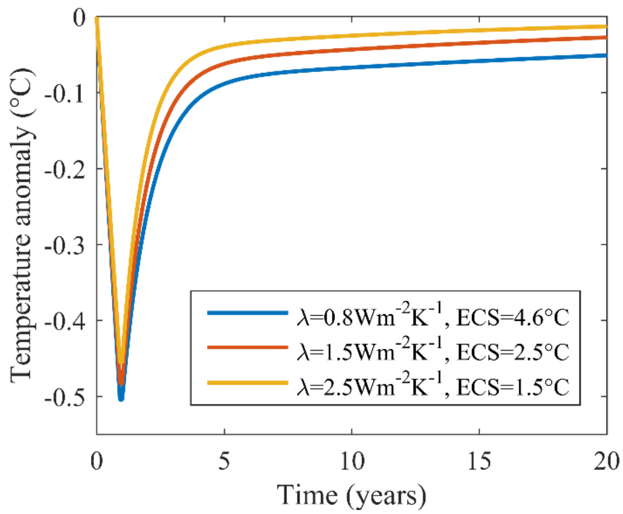

Fig. 8: 2-box model responses to an idealized Pinatubo forcing (-4 Wm^{-2} for a year) for a range of λ (or ECS) values. All other parameters are fixed to those in Table 1.

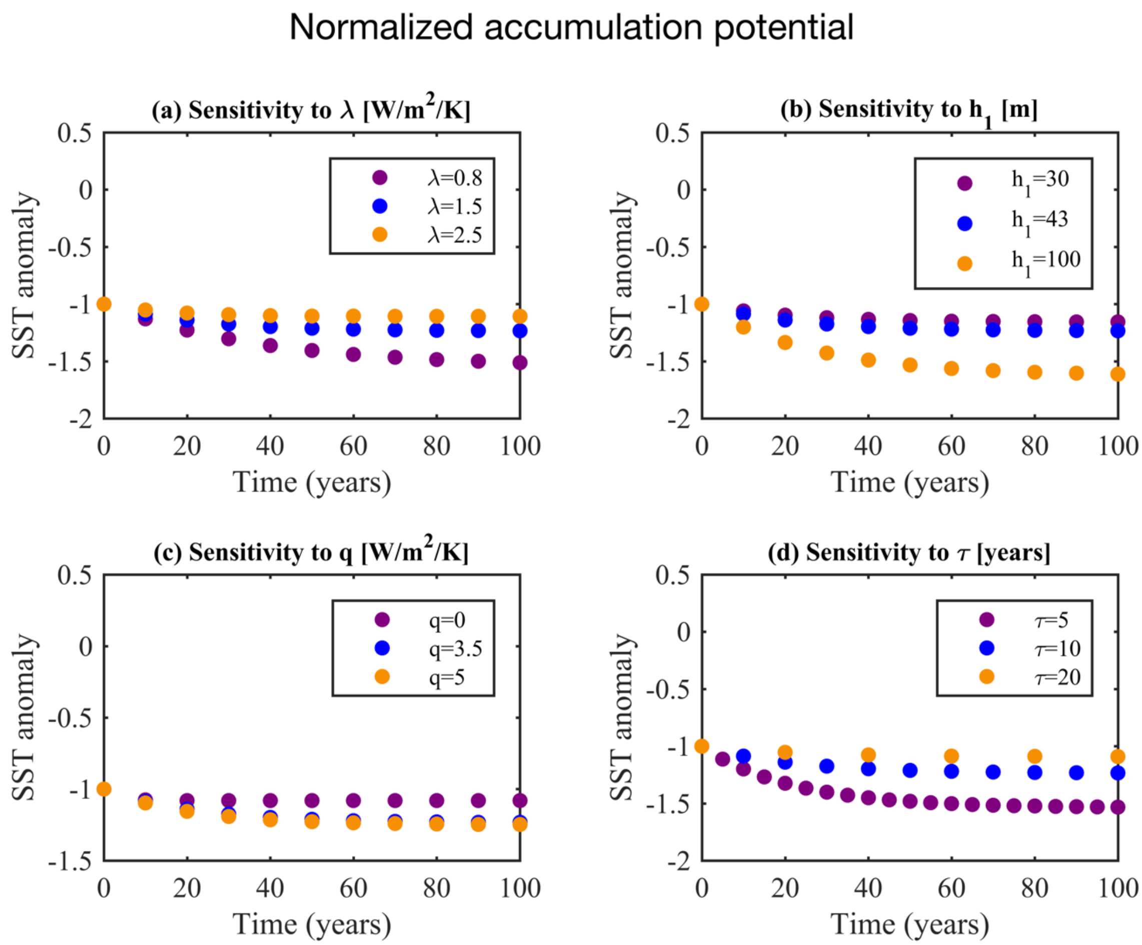

Fig. 9: Normalized temperature envelope T_{en} for a series of uniform and regularly spaced eruptions in the 2-box model. Each dot represents the peak cooling temperature after a new eruption. Parameter sensitivity is explored for (a) the climate sensitivity λ, (b) the mixed layer depth h_1, (c) the ocean exchange parameter q and (d) the time interval between eruptions τ.

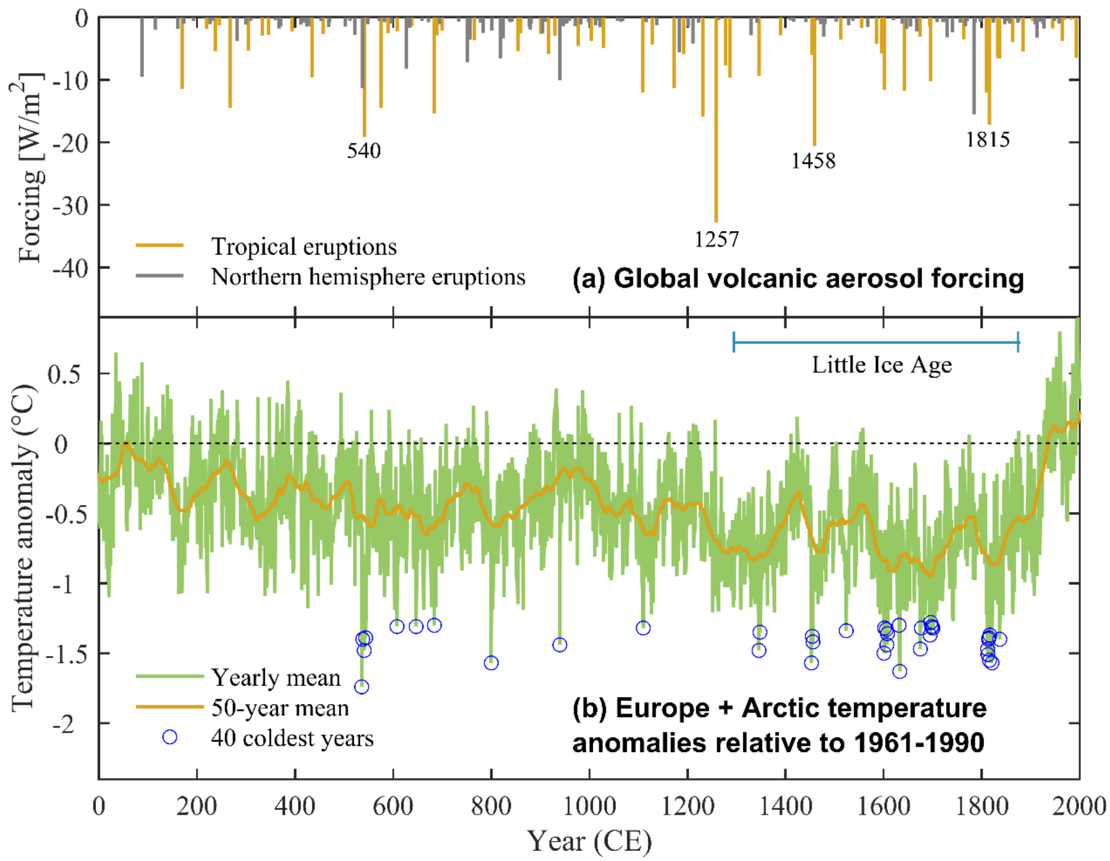

Fig. 10: (data from Sigl et al. 2015): (a) 2000-year reconstruction of global volcanic aerosol forcing from sulfate composite records from tropical (orange) and Northern Hemisphere (gray) eruptions. (b) 2000-year record of reconstructed summer temperature anomalies for Europe and the Arctic relative to 1961-1990 shown yearly (green) and as a 50-year running mean (orange). The 40 coldest single years are indicated with blue circles and the approximate duration of the Little Ice Age is shown.

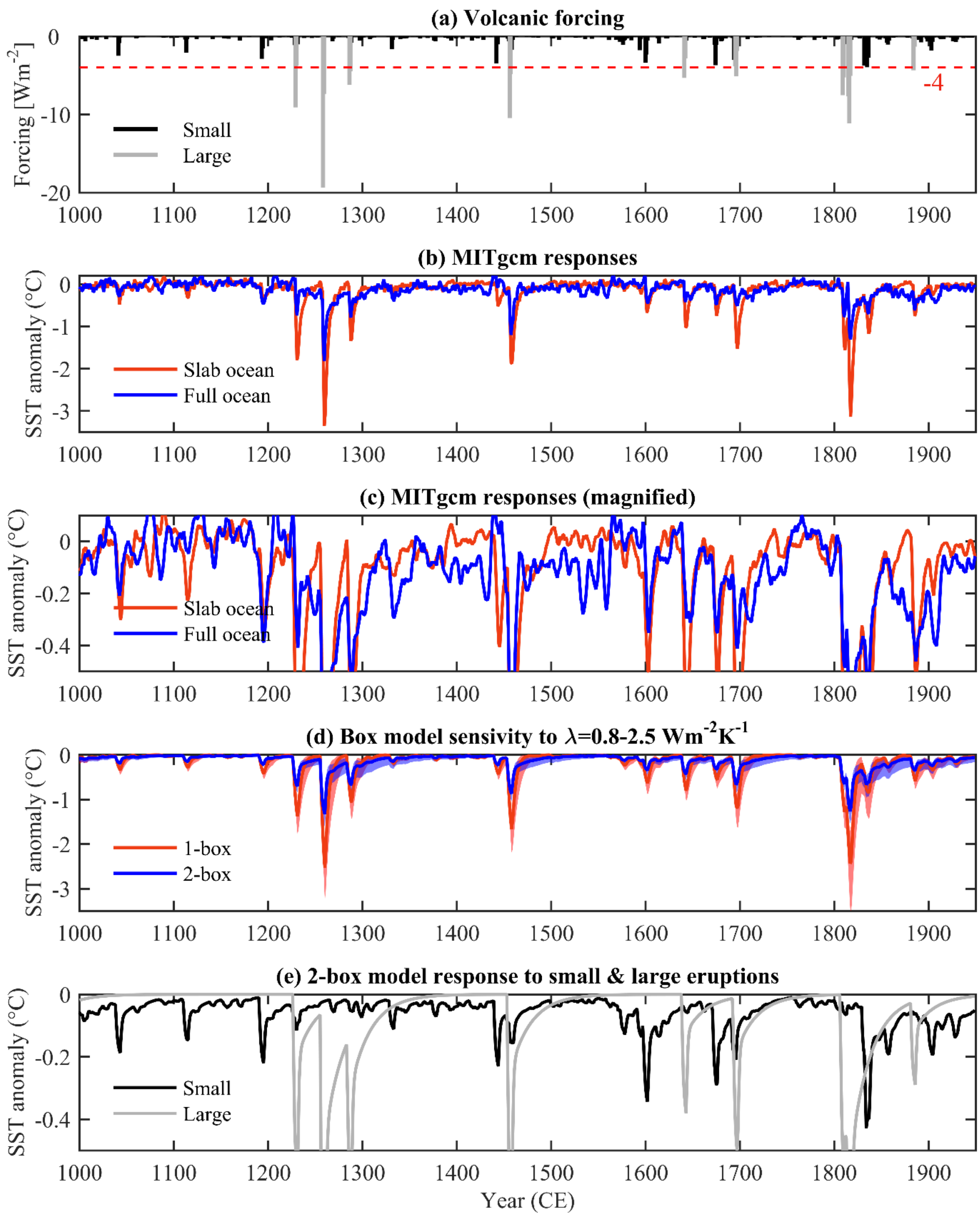

Fig. 11: (a) Tropical volcanic forcing of the last millennium (A. LeGrande, NASA GISS, personal communication) divided into small (> -4 Wm^{-2}) and large eruptions (≤ -4 Wm^{-2}). (b)

responses of the MITgcm coupled model with a full ocean (blue) and a slab ocean (red) to the volcanic forcing shown in (a). (c) 5-year running mean of (b) on a magnified scale. (d) Reconstructed response obtained by convolving the forcing in (a) with the response functions (red and blue) shown in Fig. 6 (a) and sensitivity to λ (shading). (e) 5-year running mean of the 2-box model response to the small (black) and large (gray) volcanic forcing.

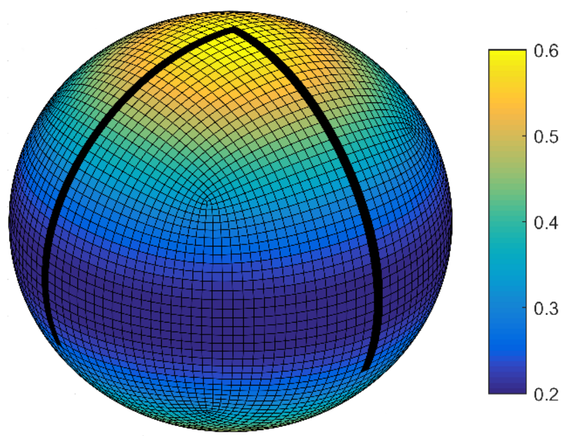

Fig. A1. Linear albedo gradient imposed at the surface of the MITgcm model. The grid is in a cubed sphere configuration with 32×32 points per face, with a nominal horizontal resolution of 2.8°. The thick black lines indicate the solid ridges of the ‘double-drake’ setup extending from the North Pole to 35°S and set 90° apart.

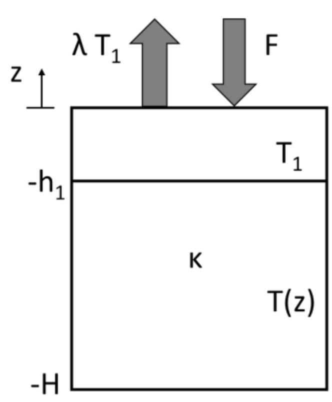

Fig. A2: 1-D diffusion model with mixed layer depth h_1, deep ocean depth H, thermal diffusivity κ, climate feedback parameter λ, mixed layer temperature T_1 and deep ocean temperature T(z).

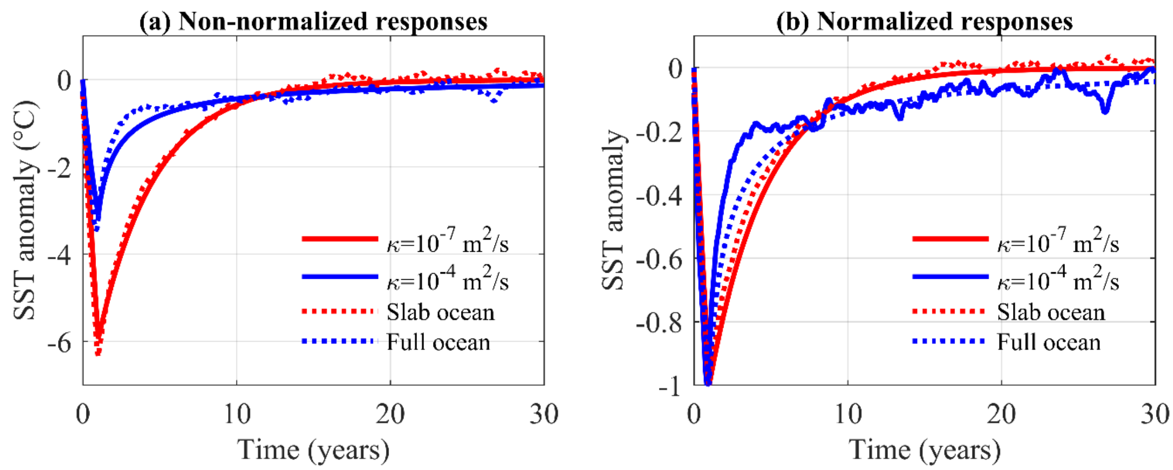

Fig. A3: Mixed layer temperature anomaly in the 1-D diffusion model (solid lines) and MITgcm (dotted lines) for a -40 $Wm^{-2}K$ pulse lasting 1 year. The red lines correspond to a slab ocean whereas the blue lines are for a full ocean. The response functions are shown for (a) non-normalized values and (b) normalized by the corresponding peak cooling value.

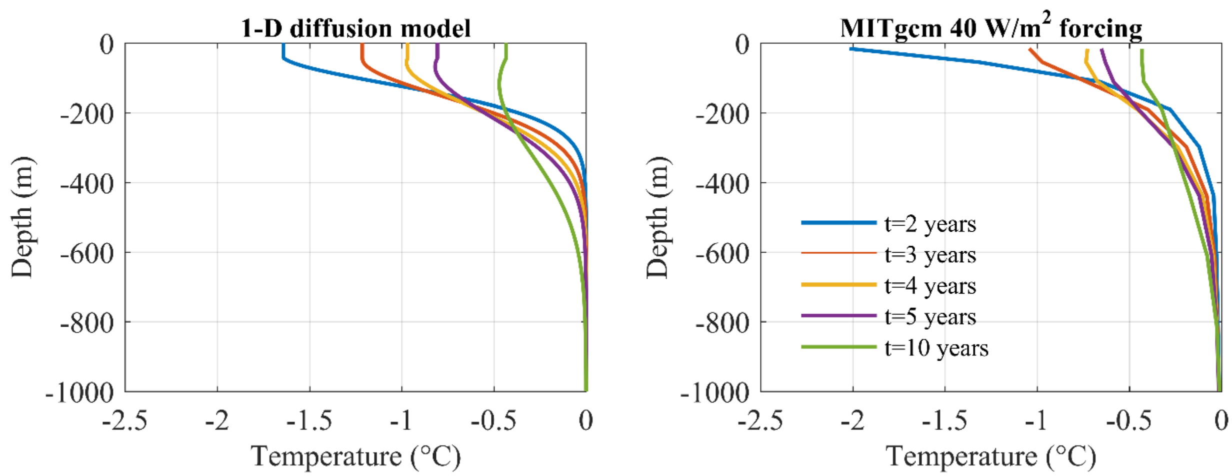

Fig. A4: Time evolution of temperature profiles with depth for a 1-year forcing of -40 Wm^{-2} in (a) the 1-D diffusion model with $\kappa = 10^{-4}\ m^2s^{-1}$ and (b) the horizontally MITgcm full ocean configuration.